



Rapid production of a ^{85}Rb Bose-Einstein condensate in a double compressible optical dipole trapHaruka Otoishi, Shu Nagata , Takumi Yukawa, Kazuya Yamashita, * and Toshiya Kinoshita †*Course of Studies on Material Science, Graduate School of Human and Environmental Studies, Kyoto University, Yoshida-nihonmatsu-cho, Sakyo-ku, Kyoto 606-8501, Japan*

(Received 11 May 2020; accepted 21 July 2020; published 18 August 2020)

We develop an all-optical method to rapidly produce a large ^{85}Rb Bose-Einstein condensate. ^{85}Rb has a reputation as a difficult species to cool to quantum degeneracy due to its collisional properties. We solve these intrinsic difficulties by a combination of polarization gradient cooling in a 3D optical lattice and a compressible double-crossed dipole trap (DCDT). This lattice cooling circumvents the low rethermalization rate and loads more than 10^7 atoms with a phase-space density larger than 10^{-3} into the enlarged DCDT. The subsequent compressions and evaporations in the size-adjustable DCDT can maximize the cooling efficiency while reducing unnecessary inelastic losses. We fix the bias magnetic field to 161 G where the s -wave scattering length is positive and large. The forced evaporations function well against inelastic collisions at an average density of $5 \times 10^{12} \text{ cm}^{-3}$. A nearly pure condensate of 2×10^5 atoms is produced in 3.2 s of evaporation time.

DOI: [10.1103/PhysRevA.102.023316](https://doi.org/10.1103/PhysRevA.102.023316)**I. INTRODUCTION**

The precise tuning of scattering lengths by a magnetic field is one of the greatest advantages of experiments with quantum degenerate gases. By using Feshbach resonances, interaction tunable Bose-Einstein condensates (BECs) have provided important experimental applications [1]. For example, negligible interactions are preferable for high-precision atomic interferometry and long-lived Bloch oscillations [2,3]. Ultracold molecules in the quantum degenerate regime have led to advances in ultracold chemistry [4,5]. The dynamics of collapsing BECs and the formation of bright solitons can only be investigated by using Feshbach resonances [6,7]. Feshbach tuning also has been applied to quantum gases in optical lattices and lower dimensional systems [8–10].

^{87}Rb has been the prevalent atomic species in BEC experiments since its first realization in a dilute gas. However, the Feshbach resonance with the largest width for the $|F m_F\rangle = |1 1\rangle$ state is located at 1007 G and even this width is only 200 mG. The interaction tuning of ^{87}Rb has been demonstrated before [11] but handling large currents with high field stability remains the biggest drawback.

On the contrary, the Feshbach resonance of ^{85}Rb is much easier to access. It is located at 155 G with a width of 10.7 G for the $|F m_F\rangle = |2 - 2\rangle$ state [12], which enables us to widely tune the s -wave scattering length on both positive and negative sides. However, its collisional properties make it difficult to cool gases to quantum degeneracy. Above hundreds of μK , the s -wave elastic cross section is two orders of magnitude smaller than that of ^{87}Rb [13]. The standard approach of directly loading the gas from a magneto-optical trap

(MOT) and adiabatically compressing the magnetic trap (MT) in succession is ineffective due to the significantly slower rethermalization. Furthermore, the two-body and three-body inelastic loss rates are very high. Despite these difficulties, the JILA group have developed a method to reach BEC [14] in which the gas is evaporatively cooled in the MT at 250 G where the s -wave scattering length a_s is negative but the inelastic loss rates are very small [15]. By shifting the bias field to 162 G ($a_s > 0$) later on, a stable BEC is created. In a different attempt, the Cornish group has constructed a hybrid trap consisting of a MT and a crossed dipole trap (CDT) [16]. A 40-s evaporation produces a pure BEC of 4×10^4 atoms during this whole process. An alternative method to produce BEC is sympathetic cooling with ^{87}Rb [17,18]. This yields the largest ^{85}Rb BEC of 8×10^4 [17] but the procedure is complex and takes a longer time than other atomic species. A common scheme employed in these methods is to shelve the atoms at a magnetic field where the inelastic loss rates are minimal and begin evaporative cooling at very low densities. However, forced evaporations take longer at lower densities and inelastic losses reduce the condensed atom number. This significantly longer time needed to reach degeneracy and the lower condensed atom number are the biggest reasons for the underutilization of ^{85}Rb . Feshbach resonances with large broadenings at high bias magnetic fields have also been investigated, but these have not been utilized for creating BECs [19]. Therefore, the efficient production of ^{85}Rb BECs has remained a challenge.

In this paper, we report on the rapid production of a pure BEC of 2×10^5 ^{85}Rb atoms using an all-optical method. We chose a method that specifically addresses the aforementioned issues that arise when cooling ^{85}Rb atoms. We bypass the issue of the low rethermalization rate by using lattice cooling, i.e., polarization gradient cooling (PGC) in a three-dimensional far-off resonant optical lattice (3D-FORL) and manage the large inelastic losses during evaporative cooling

*Present Address: Department of Physics, Graduate School of Science, Kyoto University, Kyoto 606-8502, Japan.

†kinoshita.toshiya.6x@kyoto-u.ac.jp

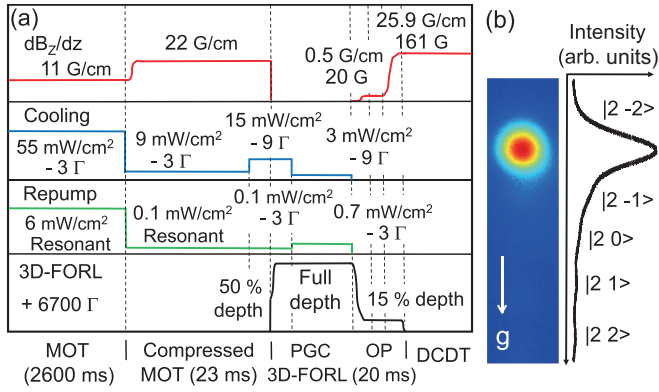


FIG. 1. (a) Time sequences of the magnetic field gradient, cooling light, repump light, and 3D-FORL during laser cooling. The detuning of cooling (repump) light is measured with respect to the $5S_{1/2} F=3 (F=2) \rightarrow 5P_{3/2} F'=4 (F'=3)$ transition. $\Gamma/2\pi = 6$ MHz. The timescale shown above in the MOT stage does not reflect the actual time. (b) High-intensity fluorescence image after optical pumping. The adiabatically released gas from the 3D-FORL expands for 30 ms in free space while being levitated by the magnetic field gradient. Infinitesimal fractions in other magnetic sublevels fall down due to gravity without being recaptured in the DCDT.

by using a compressible double crossed dipole trap (DCDT) [20]. By adiabatically turning off the 3D-FORL, we load more than 10^7 atoms with a phase-space density of 6×10^{-3} into the DCDT. The compressions and evaporations in the size-adjustable DCDT allow us to optimize the cooling efficiency while reducing unnecessary inelastic losses. Instead of the bias switching method, we fix the magnetic field at 161 G with positive $a_s = +350 a_0$ ($a_0 = 0.0529$ nm is the Bohr radius) and a relatively large elastic cross section. The forced evaporations continue to function well under inelastic collisions at a relatively high average density of $5 \times 10^{12} \text{cm}^{-3}$. This method produces a large condensate in the single CDT in only 3.2 s of evaporation time.

This paper is organized as follows. In Sec. II, we explain the laser cooling scheme before the loading into the DCDT. In Sec. III, we describe the compression and evaporation procedure in the CDTs. We present the whole sequence from the initial loading to the final BEC in Sec. IV. Finally, we summarize our results in Sec. V.

II. LASER COOLING

Our experimental setup and cooling techniques are described in Ref. [20]. The atom number N is measured by high intense fluorescence imaging [21] and the temperature is estimated by absorption imaging. The optimized sequences and parameters up to the loading into the DCDT are shown in Fig. 1. We load chirp-cooled atoms into a MOT and dynamically compress the gas by suddenly changing the MOT parameters. When the gas reaches a peak density of $7 \times 10^{11} \text{cm}^{-3}$ with 2×10^8 atoms and a temperature of $\sim 80 \mu\text{K}$, we turn off the magnetic field and turn on the 3D-FORL. We create the 3D-FORL with 40 GHz blue-detuned, three orthogonal linearly polarized standing waves with $600 \mu\text{m}$ waists. The frequencies differ from one another by 80 MHz.

Therefore, the lattice beams are linearly polarized everywhere and the 3D-FORL depth of $300 \mu\text{K}$ is sublevel independent. The vibrational level spacing is $14 \mu\text{K}$. By abruptly turning the 3D-FORL on up to its half maximum depth followed by an adiabatic ramp-up to its maximum depth, most atoms are bound to the lattice sites. Since the site occupation is typically 0.1 due to its limited atomic density in the compressed MOT, atoms no longer collide. PGC in the 3D-FORL under these conditions functions well, particularly for a dense atomic sample. This has been first demonstrated in a Cs gas as described in Refs. [22,23].

PGC is carried out by simply using the MOT and repump lights with larger detunings. For the first 3 ms, the cooling light intensity is relatively large. The 3D $\sigma^+ - \sigma^-$ lights cool atoms into the few lowest vibrational states by the Sisyphus mechanism [22,24]. The separation between the cooling and trapping lights enables us to optimize temperature independently. After 8 ms of more cooling at low intensities, we obtain the coldest gas of $15 \mu\text{K}$. Due to the weak repump lights, most atoms are in $F=2$, excluding them from the cooling cycles. Therefore, reabsorptions of spontaneously emitted photons are reduced. Atom isolation in the lattice sites and the reduced reabsorption significantly suppress density-dependent heating.

After PGC, we completely shut off the cooling and repump lights but keep the 3D-FORL turned on. The depth is decreased to $45 \mu\text{K}$ to reduce the lattice photon scattering which causes heating and depolarization. The lattice is still deep enough to hold the atoms in all directions. Next, we apply a bias field of 20 G for optical pumping. We use the σ^- polarized, weak D_1 light which is blue-detuned by 10 MHz with respect to the $5S_{1/2} F=2 \rightarrow 5P_{1/2} F'=2$ transition. In addition, a weak, π polarized light is applied to depump the atoms to $F=2$. The detuning is set to be -30 MHz from the $5S_{1/2} F=3$ to $5P_{3/2} F'=3$ transition. Both lights are illuminated for 2 ms and more than 90% of the atoms are transferred to the $|2 -2\rangle$ state as shown in Fig. 1(b). After the pumping, we ramp up the bias field to 161 G with a field gradient ($\simeq 25.9$ G/cm) to levitate the atoms against gravity. We then adiabatically turn off the 3D-FORL in $200 \mu\text{s}$. 1.5×10^8 atoms are further cooled down to $2.5 \mu\text{K}$ and released into the enlarged DCDT.

This lattice cooling does not rely on collision-assisted thermalization processes. Without any difficulty, we can easily produce a spin-polarized gas in the few μK range. An initial PSD of $\geq 10^{-3}$ is advantageous for evaporative cooling. This greatly differs from previous methods [14,16–18], where evaporation begins at much higher temperatures ($50 - 700 \mu\text{K}$) in a very weak trap, suggesting the initial PSD is $\leq 10^{-5}$. Raman-sideband cooling in a FORL, which is a key technique used to produce Cs BECs, can realize lower temperatures [25,26], but PGC in the 3D-FORL is experimentally much simpler.

III. COMPRESSION AND EVAPORATIVE COOLING

The elastic collision rate and the two- and three-body inelastic losses strongly depend on the density and the magnetic field near the Feshbach resonance. Figure 2 shows a_s and the calculated elastic cross section σ_{el} at different temperatures.

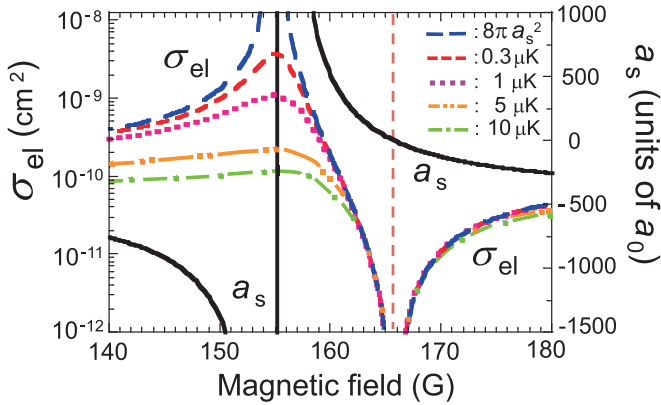


FIG. 2. Calculated elastic cross sections σ_{el} and s -wave scattering length a_s (solid black lines) near the Feshbach resonance. σ_{el} at different temperatures including the ultracold limit ($8\pi a_s^2$) are shown. The length unit of a_s is the Bohr radius $a_0 = 0.0529$ nm. a_s is given by $a_{bg}(1 - \frac{\Delta}{B-B_0})$ with $a_{bg} = -443 a_0$, $\Delta = 10.7$ G, and $B_0 = 155$ G [12]. The vertical dashed line indicates the location of $a_s = 0$.

We use a simple form of σ_{el} given by $8\pi a_s^2/(1 + k^2 a_s^2)$, where $k = (4mk_B T/\pi \hbar^2)^{1/2}$ is the relative wave number [1]. The Cornish group begins evaporations at 175–185 G where the rate coefficients for the two-body loss K_2 and the three-body loss K_3 , 10^{-14} cm 3 s $^{-1}$ and 10^{-26} cm 6 s $^{-1}$, respectively, remain close to minimal [15]. The same group has confirmed that the cooling efficiency $\gamma = -\frac{\Delta(\ln\text{PSD})}{\Delta(\ln N)}$ peaks around 180 G ($\gamma \simeq 2$) and found the slightly lower, second-largest peak ($\gamma \simeq 1.5$) between the narrow range of 160–163 G [16]. In this region, K_2 and K_3 become larger [15], but σ_{el} also increases as the bias field approaches the resonance as shown in Fig. 2. These two competing factors produce the second-largest maximum of γ . Our trap lifetime is limited to ~ 15 s due to background collisions. It may be a better choice to shorten the evaporation time by selecting a bias field in this range which we did in this paper.

Our DCDT consists of two different CDTs [20]. Both are operated at $\simeq 1.06$ μm but the trap sizes are significantly different. The larger CDT is built by a high-power multi-mode fiber laser (MCDT) and the smaller CDT is built by a single-mode fiber amplifier (SCDT). At the initial loading, the enlarged DCDT recaptures a large number of atoms from the 3D-FORL. Both are then simultaneously compressed to largely different sizes by the zoom lenses. Subsequently, the atoms are evaporatively cooled by only decreasing the MCDT power while transferring the gas into the SCDT at the same time [see Fig. 3(b)]. During this process, the tighter SCDT maintains the trap stiffness. Therefore, the cooling and transfer can be achieved efficiently in quick succession which has been demonstrated for ^{87}Rb [20]. Once the transfer is complete, the subsequent cooling and compression in the SCDT are relatively straightforward. The current setup does not allow us to adjust the two trap sizes independently. Nevertheless, the combinations of compression and evaporation could still provide many possible sequences to control elastic and inelastic collisions. We divide the sequence into multiple stages and try to optimize each process in order, which we

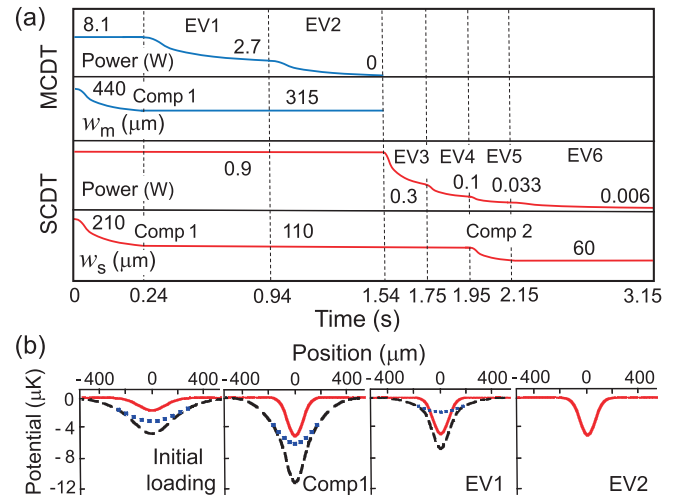


FIG. 3. (a) Optimized sequences of compressions and forced evaporations in the DCDT. The beam radii and powers of the MCDT and the SCDT are shown as functions of time, respectively. (b) DCDT potentials from the initial loading to the end of the second evaporation (EV2). The DCDT (dashed black line) is composed of the MCDT (dotted blue line) and the SCDT (solid red line). Vertical scales are the same for all plots. The evaporation and the compression continue after EV2 (not shown).

explain in detail later. The resulting optimized sequences are shown in Fig. 3(a).

First, we determine the initial trap sizes to maximize the atom number held in the DCDT for 300 ms, even though we start compression immediately after turning off the 3D-FORL. The largest atom number obtained is 1.5×10^7 where the e^{-2} radii of the MCDT is $w_m = 440$ μm and the SCDT is $w_s = 210$ μm . The total depth U is 5.5 μK , given by the sum of the depths of the MCDT and the SCDT. The initial PSD is 6×10^{-3} .

The density profile most drastically changes during the transfer into the SCDT. Therefore, it must be carefully controlled, so we focus on the optimization of the first compression (comp 1) and cooling stage. For various compressions, we observe a two- to threefold enhancement of the PSD due to unforced evaporations concomitant with the compression. However, excessive squeezing ($w_m \leq 250$ μm and $w_s \leq 80$ μm) brings almost no gain in the PSD, mainly due to the loss of atoms. In contrast, in our previous studies with ^{87}Rb , the heating and loss were not severe even when w_s and w_m were significantly reduced to a much smaller 60 μm and 160 μm , respectively, by a single-step compression from the initial sizes. Clearly, this drastic difference is due to the large inelastic losses of ^{85}Rb . We choose the beam sizes of $w_m = 315$ μm and $w_s = 110$ μm for the first compression. These were obtained from the optimization of the first two evaporation stages after comp 1, which are explained below. The temperature just after comp 1 is 3 μK , the highest during our entire compression and evaporation sequence.

The MCDT power is decreased by 1/3 in 700 ms (EV1) and subsequently turned off completely within 600 ms (EV2). To see how the increased density interferes with evaporative cooling, we intentionally hold the gas after EV1 and observe

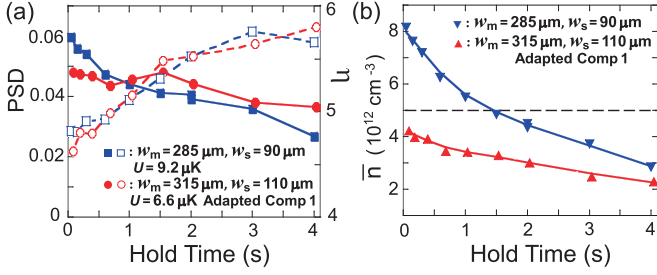


FIG. 4. Time evolution of the relevant parameters of gases after the first evaporation (EV1). (a) PSD (solid red circles and solid blue squares) and truncation parameter η (open red circles and open blue squares). (b) Average density \bar{n} . The horizontal dashed line represents $\bar{n} = 5 \times 10^{12} \text{ cm}^{-3}$. In (a) and (b), the solid and dashed lines are added as a guide. The results of two different compressions are shown with different symbols for comparison.

the time evolutions of the PSD, the truncation parameter $\eta \equiv U/k_B T$ and the average density $\bar{n} = N^{-1} \int n(\vec{r})^2 d^3\vec{r}$ and compare these results for two different trap configurations. \bar{n} is related to the peak density n_{pk} from $\bar{n} = \frac{n_{\text{pk}}}{2\sqrt{2}} = \frac{m^{3/2} N \omega_r^2 \omega_z}{(4\pi k_B T)^{3/2}}$, where ω_r and ω_z are the angular trapping frequencies in the transverse and vertical directions, respectively [27]. The results for the adapted comp 1 are shown by circles and triangles in Figs. 4(a) and 4(b), respectively. In Fig. 4(a), η exceeds 4 and keep increasing. This indicates that the gas is continuously cooled by unforced evaporations and its effect on the temperature is still larger than any possible heating caused by inelastic collisions. On the other hand, the PSD stays steady at most hold times. This strongly suggests that any positive effect the cooling has on the PSD nearly balances out the inelastic loss of atoms. The measurements in the slightly smaller DCDT are also plotted by squares and inverted triangles in Fig. 4. In this case, the cooling progresses at the same pace and the PSD right after the end of EV1 is slightly larger. However, the PSD continuously decreases for longer hold times. We confirm that the PSD after EV2 becomes smaller than that of the adapted comp 1. From the rapid reduction of the PSD and \bar{n} seen in Figs. 4(a) and 4(b), it is evident that inelastic losses become more significant in the tighter DCDT when \bar{n} exceeds $5 \times 10^{12} \text{ cm}^{-3}$. Their reduction rates for both trap configurations are slower below this density.

In the adapted comp 1 specified by the aforementioned evaporation times, we obtain the largest PSD when the atoms are completely transferred into the SCDT. The average γ from the initial loading to the end of the transfer is $\simeq 2$. The sensitivity of the compression size indicates the difficulty of selecting the beam size. Our compressible CDT allows us to adjust the trap size over time, which is a large advantage compared to a fixed-size CDT or a dimple trap.

We continue evaporation by ramping down the SCDT power by every 1/3 (EV3 – EV5). The trap stiffness is reduced and \bar{n} is kept less than $4 \times 10^{12} \text{ cm}^{-3}$. We minimize w_s to 60 μm in 200 ms (comp 2) and we complete EV5 at almost the same time. We obtain the max PSD from these procedures. The calculated \bar{n} is $5.5 \times 10^{12} \text{ cm}^{-3}$, which is quickly reduced again by the subsequent final evaporation (EV6).

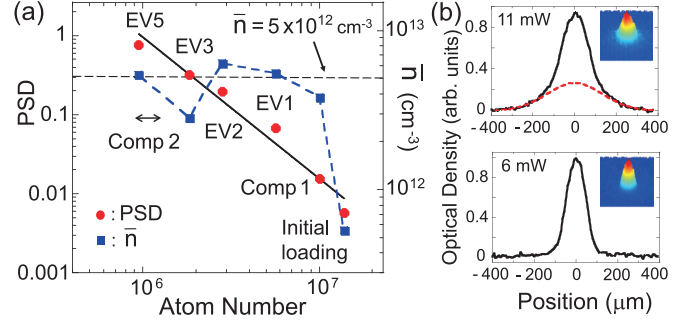


FIG. 5. Progress of the PSD on the way to reaching BEC. (a) PSD (solid circles) and the calculated average density \bar{n} (solid squares) are plotted as functions of the atom number. The solid line indicates the fitting results of the evaporation efficiency $\gamma = 1.8$. (b) Vertical cross sections of the density profiles of condensed gases after 70 ms of time of flight. Upper: 50% condensed gas. A dashed red line represents the thermal component. Lower: Nearly pure BEC. Inset shows the corresponding 3D color map image. The beam power of the SCDT is written at the top left corner.

IV. BOSE-EINSTEIN CONDENSATION

The BEC transition occurs at around $\simeq 6 \times 10^5$ atoms in the middle of EV6. A pure condensate with 2×10^5 atoms is produced at the final trap depth of 140 nK. The trapping frequencies are $\omega_r/2\pi = 19 \text{ Hz}$ and $\omega_z/2\pi = 27 \text{ Hz}$ and $n_{\text{pk}} = 2.5 \times 10^{13} \text{ cm}^{-3}$. The BEC life time is $\simeq 6 \text{ s}$ at 161 G. The evaporation time after the initial loading is 3.2 s. Figure 5(a) represents the progress of the PSD and \bar{n} . The density profiles of the condensed gases are shown in Fig. 5(b). We have optimized the sequence by maximizing the PSD for each step, except for comp 1 and EV1. This results in the overall optimization of the largest condensed number. Surprisingly, the resulting average density \bar{n} remains close to $5 \times 10^{12} \text{ cm}^{-3}$. At this density, the per-particle two-body and three-body inelastic collision rates $\Gamma_{2b} = K_2 \bar{n}$ and $\Gamma_{3b} = K_3 N^{-1} \int n(\vec{r})^3 d^3\vec{r} = \frac{8}{\sqrt{27}} K_3 \bar{n}^2$ are 0.5 s^{-1} and 3.8 s^{-1} , respectively [28]. The elastic collision rate $\Gamma_{\text{el}} = \bar{n} \sigma_{\text{el}} \bar{v}_{\text{rel}}$, where $\bar{v}_{\text{rel}} = (16k_B T/m\pi)^{1/2}$ is the average relative velocity, is $\sim 1000 \text{ s}^{-1}$ from comp 1 to EV2 and decreases to $\leq 500 \text{ s}^{-1}$ afterward. Γ_{el} is much larger than the corresponding trap frequencies of $\omega_r/2\pi = 60 - 65 \text{ Hz}$ and $\leq 45 \text{ Hz}$, respectively. According to these calculations, the gas might be in the hydrodynamic regime. In the hydrodynamic limit, the rethermalization rate of a whole sample is limited by the trap frequency [29]. However, this rate is still much higher than Γ_{2b} and Γ_{3b} . Therefore, the cooling process is unlikely to be hindered. In fact, the PSD steadily increases at each evaporation stage and an average γ of $\simeq 1.8$ is realized as shown by the solid line in Fig. 5(a). Our method strongly refutes the conventional wisdom that evaporative cooling should begin at very low densities.

At the early stages of this experiment, we tried to create a BEC using the existing bias-switching method from 177 G to 161 G. More than 10 s of evaporation yielded in a much smaller BEC with $\lesssim 2 \times 10^4$ atoms. In general, slower evaporations lead to a larger condensate, but our fast sequence fixed at 161 G allows us to rapidly enter the quantum

degenerate regime and produce a larger condensate than the existing methods.

We verify the tunable interactions in two different ways. First, we rapidly change a_s from $+350a_0$ to $+30a_0$ by increasing the bias field in 3 ms. We then observe the breathing oscillations of the atomic clouds. The mode frequency is found to be $\sim\sqrt{5}$ times the trapping frequency of the SCDT, which is in good agreement with the theory [30]. Alternatively, we alter a_s very slowly without inducing any collective excitation. The cloud sizes after time of flight decrease as the final magnetic fields increase from 161 G. The size becomes the smallest at $\simeq 166$ G. We observe the collapse of BECs above 166 G. These measurements are consistent with the crossover from the positive to negative scattering length.

V. CONCLUSION

In conclusion, we have presented an all-optical method to produce a pure BEC of 2×10^5 ^{85}Rb atoms in 3.2 s of evaporation. We have incorporated the two techniques of the 3D lattice cooling and a compressible DCDT. The lattice cooling rapidly produces a very cold, spin-polarized gas with a phase space density larger than 10^{-3} , essentially bypassing the low rethermalization rate. This significantly increases the initial atom number in the DCDT and shortens the subsequent evaporation time. We manage the inelastic loss

by a combination of compressions and evaporations in the DCDT. We fix the magnetic field at 161 G, where the s -wave scattering length is positive and large. The optimized experimental sequence is realized by rapid reductions of the trap depths. We confirm forced evaporations function well against the inelastic collisions at an average density of $5 \times 10^{12} \text{ cm}^{-3}$. The compressible DCDT allows us to adjust the trap size, which would be difficult to do with just having a single CDT. Therefore, we are able to optimize the cooling efficiency at every step along the way to reaching BEC. Both condensed atom number and evaporation time are comparable to other commonly used atomic species. Our method circumvents the largest disadvantage of ^{87}Rb , i.e., accessing the Feshbach resonance and hopefully changes the perception of ^{85}Rb as a difficult species to cool to degeneracy. This method could provide many possibilities for applications in existing Rb BEC experiments. It could also work for many other species which are difficult to condense.

ACKNOWLEDGMENTS

This work was financially supported by JSPS KAKENHI Grants No. JP26610125 and No. JP19K03685. K.Y. acknowledges financial support from JSPS (Grant-in-Aid for JSPS Fellows, JP12J00984).

-
- [1] C. Chin, R. Grimm, P. Julienne, and E. Tiesinga, *Rev. Mod. Phys.* **82**, 1225 (2010).
 - [2] M. Fattori, C. D'Errico, G. Roati, M. Zaccanti, M. Jona-Lasinio, M. Modugno, M. Inguscio, and G. Modugno, *Phys. Rev. Lett.* **100**, 080405 (2008).
 - [3] M. Gustavsson, E. Haller, M. J. Mark, J. G. Danzl, G. Rojas-Kopeinig, and H.-C. Nägerl, *Phys. Rev. Lett.* **100**, 080404 (2008).
 - [4] K.-K. Ni, S. Ospelkaus, M. H. G. de Miranda, A. Pe'er, B. Neyenhuis, J. J. Zirbel, S. Kotochigova, P. S. Julienne, D. S. Jin, and J. Ye, *Science* **322**, 231 (2008).
 - [5] F. Lang, K. Winkler, C. Strauss, R. Grimm, and J. Hecker Denschlag, *Phys. Rev. Lett.* **101**, 133005 (2008).
 - [6] E. A. Donley, N. Claussen, S. Cornish, J. Roberts, E. Cornell, and C. Wieman, *Nature* **412**, 295 (2001).
 - [7] A. Marchant, T. Billam, T. Wiles, M. Yu, S. Gardiner, and S. Cornish, *Nat. Commun.* **4**, 1865 (2013).
 - [8] E. Haller, M. Gustavsson, M. J. Mark, J. G. Danzl, R. Hart, G. Pupillo, and H.-C. Nägerl, *Science* **325**, 1224 (2009).
 - [9] J. Danzl, M. Mark, E. Haller, M. Gustavsson, R. Hart, J. Aldegunde, J. Hutson, and H.-C. Nägerl, *Nat. Phys.* **6**, 265 (2010).
 - [10] E. Haller, M. J. Mark, R. Hart, J. G. Danzl, L. Reichsöllner, V. Melezhik, P. Schmelcher, and H.-C. Nägerl, *Phys. Rev. Lett.* **104**, 153203 (2010).
 - [11] T. Volz, S. Dürr, S. Ernst, A. Marte, and G. Rempe, *Phys. Rev. A* **68**, 010702(R) (2003).
 - [12] N. R. Claussen, S. J. J. M. F. Kokkelmans, S. T. Thompson, E. A. Donley, E. Hodby, and C. E. Wieman, *Phys. Rev. A* **67**, 060701(R) (2003).
 - [13] J. P. Burke, J. L. Bohn, B. D. Esry, and C. H. Greene, *Phys. Rev. Lett.* **80**, 2097 (1998).
 - [14] S. L. Cornish, N. R. Claussen, J. L. Roberts, E. A. Cornell, and C. E. Wieman, *Phys. Rev. Lett.* **85**, 1795 (2000).
 - [15] J. L. Roberts, N. R. Claussen, S. L. Cornish, and C. E. Wieman, *Phys. Rev. Lett.* **85**, 728 (2000).
 - [16] A. L. Marchant, S. Händel, S. A. Hopkins, T. P. Wiles, and S. L. Cornish, *Phys. Rev. A* **85**, 053647 (2012).
 - [17] S. B. Papp, J. M. Pino, and C. E. Wieman, *Phys. Rev. Lett.* **101**, 040402 (2008).
 - [18] P. A. Altin, N. P. Robins, D. Doring, J. E. Debs, R. Poldy, C. Figl, and J. D. Close, *Rev. Sci. Instr.* **81**, 063103 (2010).
 - [19] C. L. Blackley, C. R. Le Sueur, J. M. Hutson, D. J. McCarron, M. P. Köppinger, H.-W. Cho, D. L. Jenkin, and S. L. Cornish, *Phys. Rev. A* **87**, 033611 (2013).
 - [20] K. Yamashita, K. Hanasaki, A. Ando, M. Takahama, and T. Kinoshita, *Phys. Rev. A* **95**, 013609 (2017).
 - [21] M. T. DePue, S. L. Winoto, D. Han, and D. S. Weiss, *Opt. Commun.* **180**, 73 (2000).
 - [22] S. L. Winoto, M. T. DePue, N. E. Bramall, and D. S. Weiss, *Phys. Rev. A* **59**, R19(R) (1999).
 - [23] M. T. DePue, C. McCormick, S. L. Winoto, S. Oliver, and D. S. Weiss, *Phys. Rev. Lett.* **82**, 2262 (1999).
 - [24] J. Dalibard and C. Cohen-Tannoudji, *J. Opt. Soc. Am. B* **6**, 2023 (1989).
 - [25] T. Weber, J. Herbig, M. Mark, H.-C. Nägerl, and R. Grimm, *Science* **299**, 232 (2003).
 - [26] C.-L. Hung, X. Zhang, N. Gemelke, and C. Chin, *Phys. Rev. A* **78**, 011604(R) (2008).

- [27] For the DCDT, we approximate ω_r to be $(\omega_{rM}^2 + \omega_{rS}^2)^{1/2}$, where ω_{rM} and ω_{rS} are the transverse angular trapping frequencies of the MCDT and the SCDT, respectively. We calculate ω_z in the same manner.
- [28] We use $K_2 = 10^{-13} \text{cm}^3 \text{s}^{-1}$ and $K_3 = 10^{-25} \text{cm}^6 \text{s}^{-1}$, taken from Refs. [15, 16].
- [29] The temperatures in this paper are measured at thermal equilibrium since the ramp-down times of the trap depths or the hold times are much longer than the trap oscillation periods.
- [30] F. Dalfovo, S. Giorgini, L. P. Pitaevskii, and S. Stringari, *Rev. Mod. Phys.* **71**, 463 (1999).